Probing the Shape and Stereochemistry of Molecular Orbitals in Locally Flexible Aromatic Chains: A Penning Ionization Electron Spectroscopy and Green's Function Study of the Electronic Structure of Biphenyl

Naoki Kishimoto, Yusuke Hagihara, and Koichi Ohno*

Department of Chemistry, Graduate School of Science, Tohoku University, Aoba-ku, Sendai 980-8578, Japan

Stefan Knippenberg, Jean-Pierre François, and Michael S. Deleuze*

Group of Theoretical Chemistry, Department SBG, Hasselt University, Agoralaan, Gebouw D, B-3590 Diepenbeek, Belgium

Received: July 5, 2005; In Final Form: August 30, 2005

We report on the results of an exhaustive study of the interplay between the valence electronic structure, the topology and reactivity of orbitals, and the molecular structure of biphenyl by means of Penning ionization electron spectroscopy in the gas phase upon collision with metastable He*(2^3S) atoms. The measurements are compared with one-particle Green's function calculations of one-electron and shake-up valence ionization spectra employing the third-order algebraic diagrammatic construction scheme [ADC(3)]. Penning ionization intensities are also analyzed by means of the exterior electron-density model and comparison with photoelectron spectra: in contrast with the lines originating from σ orbitals, ionization lines belonging to the π-band system have large Penning ionization cross sections due to their greater extent outside the molecular van der Waals surface. The involved chemi-ionization processes are further experimentally investigated using collision-energy-resolved Penning ionization electron spectroscopy. The cross sections of π-ionization bands exhibit a markedly negative collision-energy dependence and indicate that the interaction potential that prevails between the molecule and the He*(2^3S) atom is strongly attractive in the π-orbital region. On the other hand, the partial ionization cross sections pertaining to σ-ionization channels are characterized by more limited collision-energy dependencies, as a consequence of rather repulsive interactions within the σ-orbital region. A comparison of ADC(3) simulations with the Penning ionization electron spectra and UV photoelectron spectra measured by Kubota et al. [*Chem. Phys. Lett*. **1980**, *74*, 409] on thin films of biphenyl deposited at 170 and 109 K on copper demonstrates that biphenyl molecules lying at the surface of polycrystalline layers adopt predominantly a planar configuration, whereas within an amorphous sample most molecules have twisted structures similar to those prevailing in the gas phase.

I. Introduction

Biphenyl ($C_{12}H_{10}$) is composed of two phenyl rings connected by a single C−C bond. Although π conjugation tends to enforce coplanarity between these two rings, biphenyl is known to be a markedly nonplanar structure in the gas phase[1−4] due to the steric repulsion of hydrogen atoms in ortho positions. Compared with many other conjugated aromatic hydrocarbons such as benzene, *trans*-stilbene, and larger oligo-phenylene-vinylenes or polycyclic aromatic hydrocarbons, the departure from planarity must obviously strongly influence the energy distribution and shape of molecular orbitals since σ and π orbitals are allowed to directly interact as a result of the release of mirror symmetry. Biphenyl is the simplest molecule which reproduces the main structural properties of poly(*p*-phenylene) (PPP), a conjugated polymer that shows conductivity after exposure to oxidizing or reducing agents.[5] Many studies suggest that the conductivity of polymers is closely related to ionization, electron attachment, and charge-transfer excitation processes, namely, to the injection of electrons and holes into the material and the propagation of charge carriers described as electrically charged and partly localized structural distortions (polarons, bipolarons) along the polymer lattice.[5,6] Understanding in detail the relationships that prevail between the electronic structure and molecular architecture is therefore an essential prerequisite for monitoring the properties of electronic devices (field-effect transistors, electroluminescent diodes, solar cells) manufactured from such materials. The radical cations of biphenyls can be regarded as models of single-charge defects in PPP. In that respect, it is worth noting that, in the case of PPP, single-charge polarons specifically take the form of structural transitions from an aromatic to a quinoidal bonding pattern. Correspondingly, ionization of, or electron attachment on biphenyl drives the molecule toward planarity in the gas phase (twist angles of 40.1°, 18.9°, and 0.0° between the phenyl rings have been reported at the B3LYP/6-311+G(2d,2p) level for the neutral molecule and for its radical cation and anion, respectively).[7]

A further motivation for studying the electronic structure of biphenyl stems from the fact that this molecule is the base compound for polychlorinated biphenyls (PCBs),[8] which, despite their high toxicity, have served in many industrial applications as lubricating fluids, fire retardants, and insulating agents. From the impact of the location of Cl substituents onto the toxicity

* To whom correspondence should be addressed. K.O.: e-mail ohnok@qpcrkk.chem.tohoku.ac.jp. M.S.D.: e-mail michael.deleuze@uhasselt.be.

10.1021/jp053678f CCC: $30.25
Published on Web 10/29/2005

of PCBs, it appears that the latter directly relates to the structural and dynamical properties of biphenyl, namely, the relatively limited barrier to rotation about the central C−C bond (4−8 kJ mol^{-1}).[1,9] At last, from Fukui's frontier orbital theory,[10] it is clear that the topological characteristics of the HOMO and LUMO are of great significance for understanding the chemical properties and reactivity of biphenyl and similar molecules toward electrophilic or nucleophilic agents. The structural, dynamical, electronic, and chemical properties of π-conjugated systems are thus intimately related, a consideration which makes us believe that shape- and orbital-imaging techniques such as electron momentum spectroscopy[11] or Penning ionization electron spectroscopy[12] can play an essential role in the context of materials science.

The torsional potential around the central C−C bond of a nonrigid but conjugated molecule such as biphenyl has raised considerable interest on the experimental side as an important problem in structural chemistry.[7,13] For instance, various measurements (by means of Raman spectroscopy,[1] IR spectroscopy,[9] and X-ray diffraction[14]) indicate that biphenyl adopts a coplanar conformation in the solid state, which enlightens the importance of packing forces in such an environment. On the other hand, twist angles of 42−44° between the two phenyl rings have been found from electron diffraction experiments in the gas phase.[15] Besides the already reported studies of biphenyl in the gas phase by means of UV photoelectron spectroscopy,[16,17] He I UV photoelectron spectra (UPS) and Ne*($^3P_{0,2}$) Penning ionization electron spectra (PIES) of major relevance for the present study are those performed by Kubota and coworkers on films of biphenyl deposited at various temperatures on copper.[17] Irreversible changes in band intensities and energy locations were observed in both UPS and PIES upon annealing at 170 K the films obtained at a lower temperature (109 K). These intensity variations and band shifts have been interpreted as the outcome of a phase transition and realignment of the orientation of the biphenyl molecules on the metal substrate. Kubota et al.,[17] however, could not discard the possibility that these band shifts might also be due to a change in the molecular conformation.[17] Besides studying in detail the anisotropy of the interaction potentials pertaining to each ionization channel of biphenyl through detailed measurements of the collision-energy dependence of the related Penning ionization cross sections upon collision with He(2^3S), a specific goal of the present work is therefore to evaluate the influence of an enforcement of the planarity of this molecule on its Penning electron ionization and UV photoelectron spectra.

Penning ionization electron spectra (PIES) are obtained by measuring the kinetic-energy distribution of electrons that are ejected upon collision between a molecular target, M, and a rare-gas atom in a metastable excited state, A*, as a result of chemi-ionization processes for various ionization channels ($A^* + M \rightarrow A + M_i^+ + e^-$).[12] These spectra are very similar to photon-impact ionization spectra, with the essential advantage that the obtained ionization intensities represent a direct measure of the extent of the molecular orbitals outside the molecular surface (see further) and of their relative reactivity toward an approaching electrophilic agent. Therefore, Penning ionization electron spectroscopy is known as one of the most suitable methods for probing the shape and spread of molecular orbitals.

In the electron-exchange mechanism proposed for Penning ionization,[18] an electron in a molecular orbital φ_i of the molecular target M is transferred to the lowest unoccupied orbital of A* whereas the excited electron in A* is ejected into the continuum, provided A* has a larger excitation energy than the energy required for ionizing an electron in orbital φ_i. Upon neglecting through-space interactions between A* and M (see further), the excess kinetic energy of the ejected electron (in short the electron energy) is equal, in a molecular orbital (or quasi-particle) picture of ionization, to the difference between the excitation energy of the rare-gas atom and the electron-binding energy (or ionization energy, IE_i) of an electron in orbital φ_i. According to Hartree−Fock (HF) theory and Koopmans's theorem,[19] the latter binding energy is simply minus the energy of the ionized HF orbital ($-\epsilon_i$). At this level the predicted order of ionized states is very uncertain due to the neglect of many-electron interactions. A number of quasi-particle schemes exist for improving this approximation by accounting for the removal of electronic correlation induced by annihilation of a single electron in an occupied orbital and for the relaxation energy released by creation of an electron hole.[19] We refer, in particular, to the outer-valence Green's function scheme,[20] an approach that describes ionization within a quasi-particle picture through third order in the correlation potential and ensures therefore accuracies of about 0.1−0.2 eV on *vertical* one-electron ionization energies of large and low band-gap systems in the limit of an asymptotically complete basis set.[21] However, the energy released by electronic relaxation is most often largely sufficient to induce numerous electronic excitation processes within the cation, yielding to a very significant dispersion of the ionization intensity over many shake-up states with comparable intensities. This is particularly true for large π-conjugated systems.[22−24] With these systems the dispersion of intensity into many-body processes is such that for many ionization bands, both in the inner- and outer-valence regions, it is impossible to discriminate the shake-up states and the one-electron ionization states from which they originate. In such situations where the orbital picture of ionization so severely breaks down, one must resort to theoretical approaches which consistently account for both initial and final state electron correlation as well as configuration interactions in the cation. At last, EMS measurements of orbital momentum densities have recently confirmed on experimental grounds that the spread and topology of canonical molecular orbitals is very sensitive to the torsional characteristics of small molecules, such as *n*-butane.[25] In support to the newly reported gas-phase PIES and UPS measurements, another purpose of the present work is to conduct a detailed theoretical study of the one-electron and shake-up ionization bands of biphenyl in both twisted and planar configurations accounting for the structures that prevail in the gas phase and within the bulk of highly ordered (crystalline) layers, respectively.

II. Theory and Methodological Details

A. Ionization Cross Sections. In a hard-sphere depiction, the probability of the electron transfer in Penning ionization experiments and, thus, the related cross sections mainly depend on the overlaps during the collision between the lowest unoccupied orbital of A* and the ionized molecular orbital φ_i of M, outside the collision boundary surface.[26] On the basis of the electron-exchange mechanism, branching ratios of Penning ionization probabilities can be reliably studied by means of the exterior electron-density (EED) model.[26−28] In this model the exterior electron density ρ_i is calculated for individual canonical (Hartree−Fock) MOs by means of

$$\rho_i = \int_\Omega |\varphi_i(r)|^2 \, dr \tag{1}$$

where Ω is the subspace outside the repulsive molecular surface.

EED values calculated with ab initio MOs and using as repulsive molecular surface the envelope defined by rigid van der Waals spheres are known[27,28] to provide consistent insight into the relative intensities of bands in PIES. As a result of their greater extension outside the molecular van der Waals (vdW) surface, the Penning ionization cross sections of the π bands of conjugated hydrocarbons are naturally much larger than those measured for the σ bands, which the EED model easily explains.[26−28]

Electron-density contours and EED values for the relative Penning ionization cross sections have been obtained from Hartree−Fock (HF) self-consistent field (SCF) calculations performed using the 6-31++G basis set. In the contour maps shown in the sequel, thick solid curves indicate the repulsive molecular surface that has been used for evaluating the PIES cross sections in the EED model, and which is defined by atomic spheres of van der Waals radii.[29]

B. Interaction Potentials and Collision-Energy Dependence of Partial Ionization Cross Sections. According to a two-potential curve model of Penning ionization processes the electron energy (more precisely, the kinetic energy of the ejected electron, E_e^i) is equal to the energy difference, at the interdistance (R) at which the excitation transfer and chemi-ionization arise, between the incoming potential curve $V^*(R)$ for the entrance channel (A* + M) and the outgoing potential curve $V^+(R)$ for the exit channel (A + M_i^+), provided that the relative translational energy is conserved during the transfer of electronic excitation.[28,30] The position of peaks measured in PIES can be therefore analyzed as follows

$$E_e^i(R) = V^*(R) - V_i^+(R) = E_{A^*} - [IP_i(\infty) + \Delta IP_i(R)] \quad (2)$$

where E_{A^*} is the excitation energy of the atomic probe, A* (19.82 eV for He*[2^3S]), $IP_i(\infty)$ is the ionization potential for the *i*th ionization channel of the *isolated* molecule and is most commonly determined by means of UPS. At last, $\Delta IP_i(R)$ accounts for the shift in the ionization potential due to the interactions between the molecular target and the probe

$$\Delta IP_i = V^*(\infty) - V_i^+(\infty) - [V^*(R) - V_i^+(R)] \quad (3)$$

The interaction potential curves V^* describing the approach of the He*(2^3S) probe toward the molecular target along various directions have been calculated on the basis of the well-known resemblance[12b] between the He*(2^3S) and Li(2^2S) species in collision processes. It has indeed been shown that the velocity dependence of the total scattering cross section of He*(2^3S) by He, Ar, and Kr very closely matches that of Li (2^2S)[31] and that both the He*(2^3S) and Li(2^2S) probes exhibit very similar interaction potentials with various targets,[32,33] both in terms of the location and depth of the interaction well. With regard to these findings and the difficulties arising with calculations of potential-energy surfaces for excited states, the Li(2^2S) atom is most commonly used in place of the He*(2^3S) atom. The interaction potentials between the molecular target and the incoming He*(2^3S) atom have thus been calculated in this work using a model Li(2^2S) probe at the level of second-order Møller−Plesset perturbation theory (MP2)[19] in conjunction with the 6-31G basis set.[19]

Such calculations of interaction potentials are essential for qualitatively unraveling the dependence upon the collision energies of the partial ionization cross section (CEDPICS) measured from collision-energy-resolved Penning ionization electron spectra (CERPIES). Indeed, the collision-energy dependence of these cross sections [$\sigma(E_c)$] can be expressed[12b,34−36] as

$$\log \sigma(E_c) \propto (-2/s) \log E_c \quad (4)$$

when the long-range attractive part of the interaction potential V^* is dominant and of the form

$$V^*(R) \propto R^{-s} \quad (5)$$

In eq 5 the s parameter relates to the collision-energy ionization dependence of the partial ionization cross sections in PIES via $s = -2/m$ for atomic targets, with m being the slope parameter characterizing the linear regression of $\sigma(E_c)$ as a function of $\log(E_c)$. These equations show that, when the interaction potential for the entrance channel is attractive, the measured cross sections decrease as the collision energy increases: the higher the kinetic energy of the impinging metastable He* atoms, the lower the extent of the deflections of the trajectories of these species within an attractive potential well. On the contrary, if the entrance interaction potential is repulsive, the measured cross section $\sigma(E_c)$ increases with the collision energy, E_c. This is because in such a situation faster He* atoms can more deeply poke into the target molecular orbital. From a more quantitative viewpoint, it is known[12b,35,36] that in this case the slope parameter m relates to the effective decay parameter d for the repulsive interaction potential [$V^*(R) = B \exp(-dR)$], where R represents the distance between the metastable atomic probe and a target molecule and the effective parameter b for the transition probability [$W(R) = C \exp(-bR)$] through the relation

$$m = (b/d) - 1/2 \quad (6)$$

Here, the effective parameter b derives from the first ionization potential[37,38] [$I(M)$] via

$$b = 2\{2I(M)\}^{1/2} \quad (7)$$

Thus, the slope of the correlation of $\log \sigma(E_c)$ vs $\log(E_c)$ provides an effective measure of the attractivity ($m < 0$) or repulsivity ($m > 0$) of a specific MO region of the target molecule toward an electrophilic He(2^3S) species.

C. Ionization Spectra. The valence one-electron and 2h-1p (two-hole, one-particle) shake-up ionization bands of biphenyl in model twisted and planar configurations have been calculated using the so-called third-order algebraic diagrammatic construction scheme [ADC(3)][39−41] derived within the framework of one-particle Green's function (or one-electron propagator) theory.[42−45] In contrast with CI treatments of the same order in correlation, ADC(3) offers the key advantage of size consistency in the dissociation limit.[46] The size intensivity of the computed ionization energies follows readily for large (extended) systems, provided that static self-energies are obtained from charge-consistent one-electron densities.[46,47]

At the ADC(3) level, the one-electron (1h) and shake-up (2h-1p) ionization energies are recovered through third- and first-order in correlation, respectively. Except for the outermost ionization lines which appear to be extremely sensitive to the quality of the basis set,[21] ADC(3) calculations in conjunction with Dunning's correlation-consistent polarized valence basis set of double-ζ quality (cc-pVDZ)[48] are sufficient to ensure accuracies of about 0.2 eV on *vertical* one-electron ionization energies provided that the employed geometries also account for the effect of electronic correlation.[21,24a]

The ADC(3) computations described in this work have therefore been performed on molecular geometries that have

been optimized under the constraints of D_2 and D_{2h} symmetry point groups using the cc-pVDZ basis set, and density functional theory (DFT) in conjunction with the nonlocal hybrid and gradient-corrected Becke three-parameter Lee−Yang−Parr functional (B3LYP)[49] (an approach which is known to provide structural results of quality comparable to that achieved at the benchmark CCSD(T) theoretical level[23c,50]).

All the ADC(3) calculations have been carried out using the original 1p-GF/ADC(3) package of programs, interfaced to GAMESS.[51] In the present work, a threshold on pole strengths of 0.005 has been retained in the final diagonalization step, which has been performed using the block-diagonalization procedure.[52] The assumption of frozen core electrons has been used throughout, and the full molecular symmetry point group has been exploited. The convergence of the ADC(3) ionization spectra with regard to further improvements of the cc-pVDZ basis set has been rechecked by comparison with results and simulations obtained using the 6-31G and 6-31G* standard basis sets.[53] This comparison fully confirms the conclusions drawn in refs 24a and b about the influence of the basis set in ADC-(3) calculations on relatively large and strongly conjugated molecules such as naphthalene and azulene and will therefore not be repeated here.

For the sake of comparison, these computations will be supplemented by outer-valence Green's function (OVGF)[20] calculations of one-electron ionization energies, also in conjunction with the cc-pVDZ basis set. These OVGF calculations have been completed by means of the semi-direct and integral-driven algorithms implemented within the GAUSSIAN98 package of programs.[54]

In the sequel, the UV photoelectron and Penning ionization electron measurements are compared with convolutions drawn from the ADC(3) ionization spectra using as spread function a combination of a Lorentzian and Gaussian with equal weight and width (fwhm = 0.5 eV). For UPS, cross-section effects are neglected, i.e., the line intensities are simply scaled according to the pole strengths (Γ_i) computed from the 1h and 1p components of the ADC(3) eigenvectors. In contrast, line intensities in the simulated PIES have been rescaled according to the computed EED values.

III. Experimental Section

The experimental apparatus for He*(2^3S) PIES and He I UPS has been reported previously.[34,35,55] In our experimental set up, beams of metastable and electronically excited He*(2^1S, 2^3S) atoms were produced by a discharge nozzle source with a tantalum hollow cathode. The He*(2^1S) component was quenched by a water-cooled helium discharge lamp, and the He*(2^3S) (E_A = 19.82 eV) beam was introduced into the reaction cell. He I UPS were measured using the He I resonance photons (584 Å, 21.22 eV) produced by a discharge in pure helium gas. The background pressure in a reaction chamber was on the order of 10^{-7} Torr. The solid sample molecules were put into a small container under the reaction cell in the vacuum chamber at room temperature. The kinetic energy of ejected electrons was measured by a hemispherical electrostatic deflection-type analyzer using an electron collection angle of 90° relative to the incident He*(2^3S) or photon beam. Measurement of the full-width at half-maximum (fwhm) of the $Ar^+(^2P_{3/2})$ peak in the He I UPS led to an estimate of 60 meV for the energy resolution of the electron energy analyzer. The transmission efficiency curve of the electron energy analyzer was determined by comparing our UPS data of some molecules with those by Gardner and Samson[56] and Kimura et al.[57] Calibration of the electron energy scale was made by reference to the lowest ionic state of N_2 mixed with the sample molecule.

The collisional reaction dynamics of Penning ionization processes and details of the interaction potential between He* probes and target molecules can be experimentally studied by ionic counts as a function of the collision energy (E_c).[12b] For atomic targets characterized by isotropic interaction potentials, measurements of the collision-energy dependence of total ionization cross sections are amply sufficient for analyzing the dynamics of the Penning ionization process.[33] In contrast, with molecular targets the interaction potentials with the approaching probe is obviously anisotropic and only an average potential can be deduced from the collision-energy dependence of the total ionization cross section.[58] In this case, to obtain more specific information on the angular dependence of the interaction potentials within the MO region where the electron-exchange Penning ionization process occurs, one must resort to ionic-state-selected measurements of the collision-energy dependence of partial Penning ionization cross sections (CEDPICS).[34] Two-dimensional (collision-energy/electron-energy-resolved) mapping of the Penning ionization electron spectrum (2D-PIES)[35] can be achieved by combining a kinetic analysis of the ionized electrons with CEDPICS measurements employing the cross-correlation time-of-flight method[59] in order to select and monitor the velocity of the He* beam. The collision-energy dependence of PIES can strongly vary depending on the ionization channel and enables therefore rather straightforward assignments of the involved orbitals in many situations, among which in studies of five-membered (pyrrole, furan, thiophene, and bromothiophenes)[60,61] and six-membered (benzene[55,62,63] and azabenzenes[64]) conjugated cyclic compounds. For such systems, $\pi-\pi^*$ shake-up bands are known to have relatively large cross sections in PIES.[55,60−65] Their origin has been confirmed by the dependence of the related partial ionization cross section upon the collision energy, which is very similar to that of the π one-electron ionization bands to which they borrow their intensity.[55,60−64]

In the experimental setup for the collision-energy-resolved Penning ionization measurements, the metastable atom beam was modulated by a pseudorandom chopper[59] and then introduced into a reaction cell located at 504 mm downstream from the chopper disk. For reducing the resonance in chopper rotation, we attached two chopper plates to the motor and rotated these at 400 Hz. The measured Penning ionization spectra $I_e(E_e, t)$ were stored as a function of the electron kinetic energy (E_e) and time (t). The resolution of the analyzer was lowered to 250 meV in order to obtain higher counting rates of Penning electrons. Analysis of the time-dependent Penning ionization spectra $I_e(E_e, t)$ by means of the Hadamard transformation,[59] normalized by the velocity distribution of the He* beam, can lead to a two-dimensional mapping of the Penning ionization cross section as a function $[\sigma(E_e, E_c)]$ of the electron energies, E_e, and collision energies, E_c. The velocity distribution in the metastable atom beam was determined by monitoring secondary electrons emitted from a stainless steel plate inserted in the reaction cell.

IV. Results and Discussion

A. ADC(3) Analysis of the He I UPS and He*(2^3S) PIES Gas-Phase Measurements. The gas-phase UV (He I) photoelectron and He*(2^3S) Penning ionization spectra of biphenyl are displayed in Figure 1 together with a simulation of the PIES records drawn from the ADC(3)/cc-pVDZ ionization spectrum computed for the B3LYP/cc-pVDZ energy minimum form of

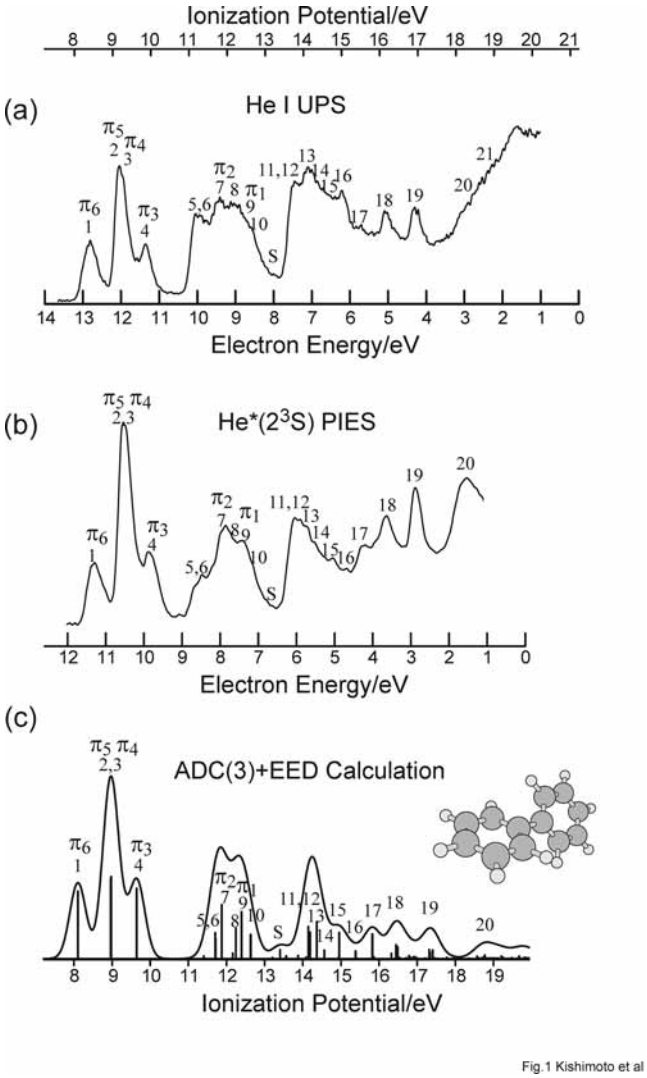

Figure 1. Comparison of the He I UV photoelectron and He*(2^3S) Penning ionization spectra of biphenyl with a simulation drawn from the theoretical ADC(3) eigenspectra and model EED cross sections calculated for the twisted (D_2) form.

biphenyl and using model EED cross sections. Despite the rather approximate nature of the EED model, the shape and relative intensities of bands in the Penning ionization electron spectrum are overall very satisfactorily reproduced by the simulation, an observation which confirms the ability of this technique to probe the spread, i.e., the σ-like or π-like character, and nucleophilicity of the molecular orbitals of large conjugated molecules, even when these exhibit significant departures from planarity. Despite the release of mirror symmetry and a twist angle of about 40° between the two phenyl rings, six of the nine outermost orbitals of the D_2 form of biphenyl (**1**, $9b_2$; **2**, 12a; **3**, $11b_1$; **4**, $9b_3$; **7**, $8b_2$; **9**, $7b_3$) exhibit markedly larger EED values, all above 4.6. These orbitals display a nodal surface that approximately follows the planes of the phenyl rings and correlate with the $2b_{2g}$, $1a_{1u}$, $1b_{1g}$, $2b_{3u}$, $1b_{2g}$, and $1b_{3u}$ π levels, respectively, of the first-order saddle-point and strictly planar form (D_{2h}) of biphenyl (Figure 2). In contrast, the remaining orbitals in the D_2 form all have EED values smaller than 2.5 and are merely localized around the C−C or C−H bonds. It can thus be concluded that these orbitals are of σ-like nature, in full agreement with the MO correlation diagram of Figure 2. For the sake of simplicity and conciseness and although such a partition is clearly abusive from a formal symmetry viewpoint, we will therefore discuss the electronic structure and ionization spectra of the energy

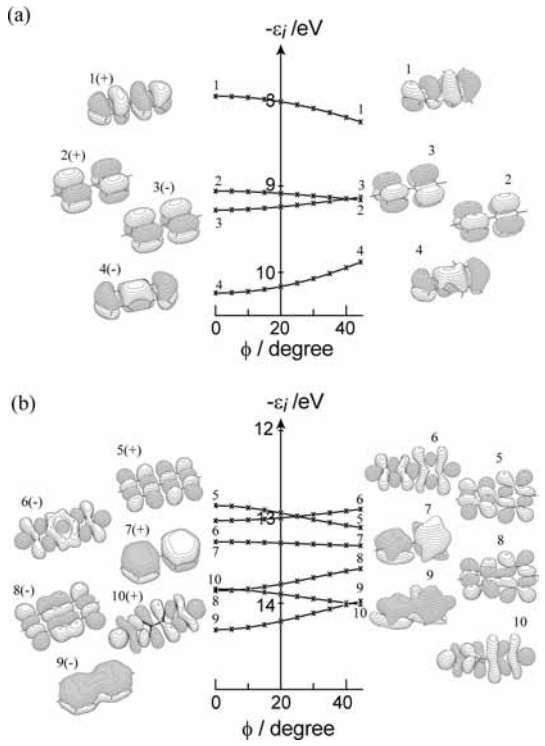

Figure 2. HF/cc-pVDZ energies of the outer-valence molecular orbitals of biphenyl as a function of the twist angles between the two phenyl rings. The provided labels are consistent with the MO assignment of Tables 1 and 2, with the spike spectra displayed in Figures 3 and 8, and with the detailed ADC(3) data provided as Supporting Information. On the left-hand-side (D_{2h} form) all levels with a_u, b_{1u}, b_{2g}, and b_{3g} symmetry labels are marked by (+), whereas all orbitals with a (−) sign relate to levels with a_g, b_{1g}, b_{2u}, and b_{3u} symmetry labels.

minimum form (D_2) of biphenyl in terms of π and σ levels according to the EED values displayed in Table 1 and the MO correlations of Figure 2. It can further be noticed from Figure 2 that all orbitals belonging to the a_u, b_{1u}, b_{2g}, and b_{3g} irreducible representations of the D_{2h} point group get stabilized by a few tenths of an electronvolt as the twist angle between the two phenyl rings increases from 0° to 42° whereas all levels with a_g, b_{1g}, b_{2u}, and b_{3u} symmetry labels are inversely destabilized (The two groups of orbitals are differentiated in Figure 2 by adding a (+) or (−) to the MO label, respectively). These energy variations obviously relate to an enhancement of through-space bonding and antibonding interactions, respectively, between the two phenyl rings and reflects the rather strongly conjugated nature of the biphenyl molecule.

The reader is referred to Table 1 for a detailed assignment of the experimental records on the basis of OVGF one-electron ionization energies and of the most important ADC(3)/cc-pVDZ results. This table confirms the empirical rule[24b,24c,66] that OVGF pole strengths smaller than 0.85 systematically corroborate a breakdown of the orbital picture of ionization at the ADC(3) level. As in previous studies of benzene and polycyclic aromatic hydrocarbons,[24] we note that the ionization bands belonging to the π-band system are subject to shake-up fragmentation at low binding energies. For biphenyl, the shake-up onset relating to the $HOMO^{-2}$ $LUMO^{+1}$ ($9b_2^{-2}$ $10b_3^{+1}$) excited configuration of the cation is a satellite at 11.42 eV ($\Gamma = 0.03$) of the $9b_3^{-1}$ (**4**) one-electron ionization line. The orbital picture of ionization partly breaks down for the two lowest π orbitals, $8b_2$ and $7b_3$ (see lines with labels **7** and **9**, respectively, in the theoretical simulations of Figures 1 and 3). In contrast, the orbital picture holds to a much greater extent within the σ-band system (namely, in this case, up to binding energies around 16 eV).

TABLE 1: Assignment of the Penning Ionization Electron Spectrum of Biphenyl, from EED Values (%), CEDPICS Slope Parameters (*m*) and by Comparison with the Ultraviolet Photoelectron Spectrum (UPS) and Theoretical [ADC(3), OVGF, and Koopmans] Ionization Energies (ADC(3) and OVGF pole strengths are given in parentheses)[a]

band	IP_{UPS}	MO	$IP_{ADC(3)/cc-pVDZ}$[b]	$IP_{OVGF/cc-pVDZ}$	$IP_{HF/cc-pVDZ}$	EED	m
1	8.41	$9b_2$ (π_6)	8.12 (0.873)	8.02 (0.890)	8.12	4.85	−0.34
2,3	9.16	12a (π_5)	8.98 (0.867)	8.80 (0.888)	9.11	5.77	−0.45
		$11b_1$ (π_4)	8.99 (0.868)	8.88 (0.887)	9.08	5.95	
4	9.87	$9b_3$ (π_3)	9.66 (0.847)	9.41 (0.886)	9.88	5.22	−0.42
5,6	11.25	$8b_3$	11.72 (0.881)	11.55 (0.893)	13.08	1.85	−0.12
		11a	11.73 (0.886)	11.40 (0.892)	13.10	1.35	
7	11.80	$8b_2$ (π_2)	11.89 (0.687), 12.18 (0.070), 16.34 (0.067)	11.78 (0.824)	13.18	4.95	−0.41
8	12.18	$7b_2$	12.26 (0.847)	12.08 (0.889)	13.62	2.25	
9	12.4	$7b_3$ (π_1)	12.41 (0.638)	12.31 (0.818)	13.86	4.63	−0.42
10	12.7	$10b_1$	12.65 (0.870)	12.46 (0.887)	14.08	1.75	
S	(∼13.2)	$7b_3$ (π_1)	13.42 (0.121)			4.63	−0.40
11,12	13.8	$6b_3$	14.16 (0.830)	14.01 (0.878)	15.74	2.43	−0.11
		10a	14.21 (0.852)	13.94 (0.877)	15.79	1.94	
13	14.11	$6b_2$	14.38 (0.851)	14.21 (0.879)	15.96	2.71	−0.23
14	14.5	$5b_3$	14.58 (0.812)	14.20 (0.864)	16.36	0.65	
15	14.7	$9b_1$	14.97 (0.843)	14.92 (0.871)	16.69	1.94	−0.22
16	15.02	$5b_2$	15.40 (0.814)	14.99 (0.861)	17.21	0.58	
17	15.53	9a	15.84 (0.810)	15.76 (0.857)	17.78	1.92	−0.26
18	16.15	$8b_1$	16.46 (0.414), 16.50 (0.360)	16.32 (0.849)	18.37	2.09	−0.25
19	16.90	8a	17.33 (0.278), 17.35 (0.190), 17.42 (0.258)	17.13 (0.840)	19.33	2.09	−0.20

[a] See Supporting Information for a more detailed description of the above ADC(3)/cc-pVDZ ionization spectrum and comparison with ADC(3)/6-31G and ADC(3)/6-31G* results. [b] Further ionization lines with pole strengths larger than 0.050 have been identified as follows. $7b_1$: 18.58 (0.152), 18.71 (0.054), 18.74 (0.084), 18.79 (0.214). $4b_3$: 19.22 (0.181), 19.26 (0.107), 19.50 (0.061). $4b_2$: 19.69 (0.159), 19.83 (0.081), 19.86 (0.058), 19.98 (0.075), 20.36 (0.063). 7a: 19.69 (0.091), 19.89 (0.060), 20.28 (0.111), 20.80 (0.061).

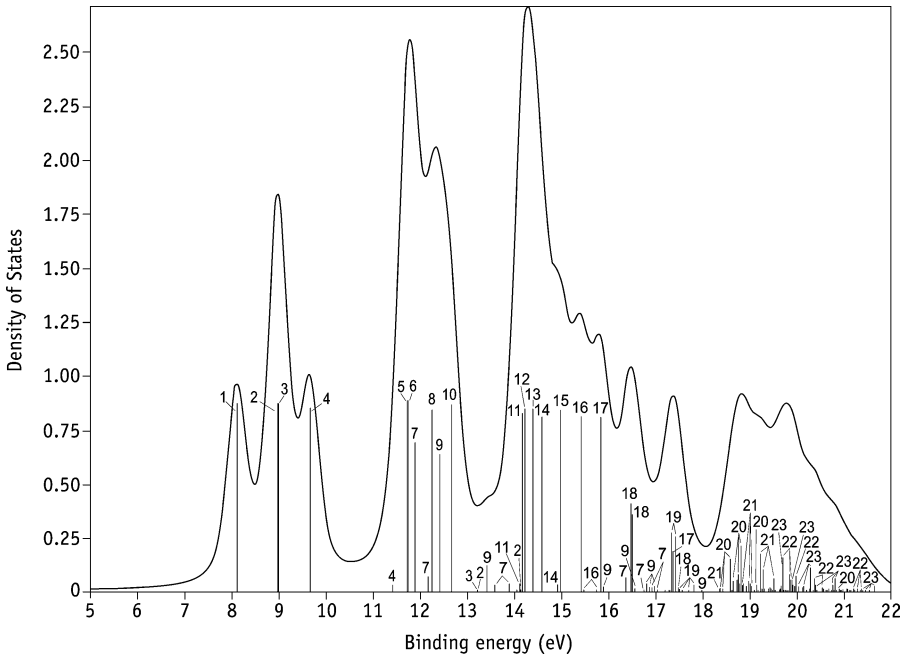

Figure 3. ADC(3)/cc-pVDZ ionization spectrum of the twisted energy minimum form (D_2) of biphenyl (spike spectra and convoluted densities of states as a function of binding energies): 21 = $4b_3$, 22 = $4b_2$, 23 = 7a. See Table 1 for a detailed orbital assignment and the available Supporting Information for a comparison with ADC(3)/6-31G and ADC(3)/6-31G* simulations.

The UPS measurements of Figure 1a can be readily compared with the ADC(3)/cc-pVDZ spike ionization spectrum and convoluted density of states calculated for that structure, which are presented in Figure 3. Overall, this convolution rather nicely matches the UPS record up to binding energies of 18 eV.

The orbital picture of ionization completely breaks down at binding energies above 18 eV. On the theoretical side, one broad peak is observed at a binding energy around 18.7 eV, in qualitative agreement with the PIES measurements. It is worth noting that, at the MP2/aug-cc-pVDZ level, the vertical and adiabatic double-ionization potentials of biphenyl amount to 21.4 and 20.8 eV, respectively. Therefore, all computed shake-up states at binding energies above 20.8 eV are subject to decay via ionization of a second electron and should be regarded as resonances in a continuum of shake-off states.

The three outermost bands in the UPS and PIES measurements are to be ascribed to four π orbitals (π_6−π_3) originating from the highest occupied MOs ($1e_{1g}$) of benzene. These energy levels display large intensities in PIES. Intensities and bandwidths in UPS and PIES also readily image the near-energy degeneracy of the π_4 and π_5 orbitals [12a (**2**) and $11b_1$ (**3**)]. In line with the EED values, this pair of lines has an extremely large intensity in PIES. In contrast, although the one-hole states produced by ionization of orbitals **5** ($8b_3$) and **6** (11a) are also quasi-degenerate, their signal emerges with much less intensity in PIES, which undoubtedly demonstrates that these orbitals

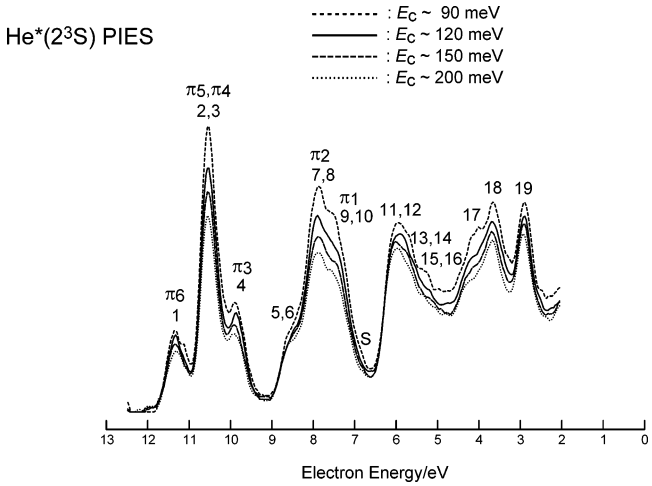

Figure 4. Collision-energy-resolved Penning ionization electron spectra of biphenyl with He*(2^3S) metastable atoms (dashed curve: E_c = 90 (±7) meV, solid curve: E_c = 120 (±12) meV, broken curve: E_c = 150 (±16) meV, dotted curve: E_c = 200 (±25) meV).

belong to the σ-band system. In straightforward analogy with the $^2E_{1g}$ (σ) and $^2A_{2u}$ (π) electronic states of the benzene radical cation, whose vibronic couplings led to a particularly complicated vibronic structure at electron-binding energies ranging from 11.4 to 12.5 eV in the UPS spectrum of this compound [see, in particular, refs 67], severe vibronic coupling interactions for ionization of an electron of the σ orbitals **5** ($8b_3$) and **6** (11a) are also expected due to the very nearby presence of a π one-electron ionization line for orbital $8b_2$ (**7**). These probably explain the poorer agreement between theory and experiment, UPS in particular, at ionization energies around 11.5 eV. This π state directly derives from the $1a_{2u}$ π orbital of benzene and can be distinctly identified in both the gas-phase UPS and the PIES measurements (Figures 1a and 1b). In line with its belonging to the π-band system, this state is more strikingly apparent in the latter case (Figure 1b).

The same consideration applies for the most intense line produced by ionization of the innermost π orbital [$7b_3$ (**9**), IP = 12.4 eV, Γ = 0.63]: this line undoubtedly relates to the peak that can be distinctly observed at an electron energy of 7.48 eV [i.e., at an ionization energy of 12.34 eV in the gas-phase PIE spectrum (Figure 1b)]. A shoulder (S) with relatively limited intensity can be discerned at an electron-binding energy of about 13.4 eV in both the UPS and PIES measurements of Figure 1a and 1b and may, at first glance, be ascribed to the vibrational tail of the π and σ orbitals **9** ($7b_3$) and **10** ($10b_1$). The EED simulation for the twisted (D_2) form of biphenyl in Figure 2b suggests that this shoulder might also relate to a rather weak $\pi^{-2}\pi^{*+1}$ satellite (S) with a pole strength of Γ = 0.12.

The next spectral feature predicted in the simulations given in Figure 3 is a sharp and narrow peak around 14.1 eV. This peak is produced by overlap of four one-electron σ-ionization lines (**11**−**14**), among which a quasi-degenerate pair (within 0.06 eV) of cationic states (**11**, **12**: $6b_3^{-1}$, $10a^{-1}$). With regard to these energy degeneracies, strong vibronic coupling effects can again be expected. Quite naturally, therefore, the bands from the σ-ionization lines (**11**−**14**) display a somewhat different appearance on the experimental side, in particular, with UPS, a spectroscopic method which by virtue of its relatively large time scale ($\sim 10^{-12}$ s) is particularly sensitive to such effects. Lower PIES intensities relative to the UPS ones suggest that bands **14** and **16** relate to one-electron ionization lines derived from σ orbitals ($5b_3$ and $5b_2$), which are merely localized around C−C bonds. Such orbitals are not easily accessible to an incoming

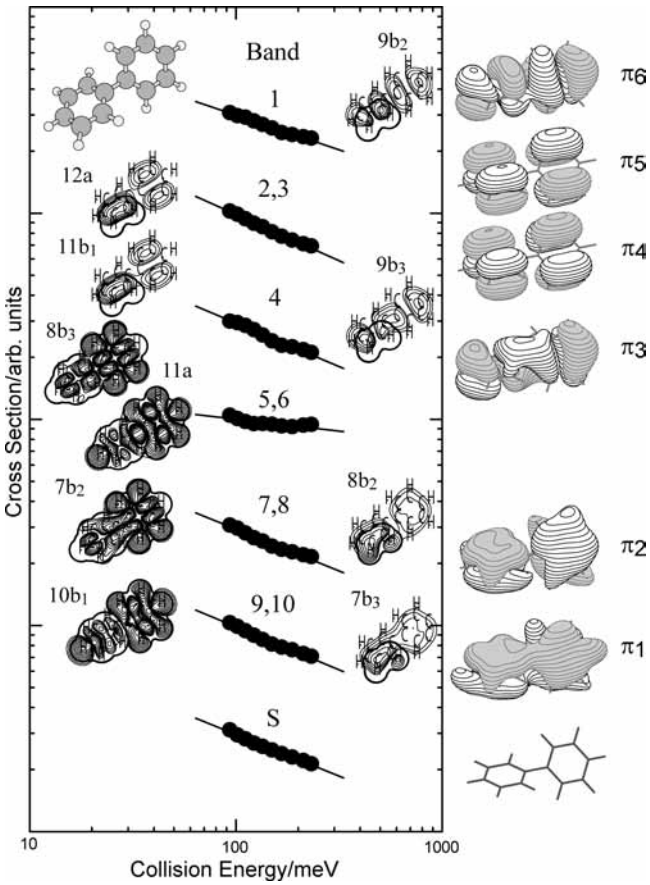

Figure 5. Collision-energy dependence of partial ionization cross sections of biphenyl with He*(2^3S) metastable atoms for bands 1−10 and band S.

He* probe and are therefore characterized by very limited EED values, smaller than 0.65. A very considerable decrease of intensity is correspondingly noted at electron energies around 5.0 eV in He*(2^3S) PIES (Figure 1b), compared with the intensity measured at ionization energies of about 14.8 eV in UPS (Figure 1a). On the other hand, orbitals **15**, **17**, and **18** ($9b_1$, 9a, and $8b_1$) are merely localized around C−H bonds. These orbitals are intrinsically more easily reachable, and larger relative EED cross sections (around 2) have been therefore calculated. This is in qualitative agreement with the PIES measurements, taking into account the presence of an intense background signal at electron energies lower than ca. 5 eV. It is worth noting that MO **17** (9a) relates exclusively to C−H contributions (see the MO plot of Figure 2). Ionization of this orbital is thought therefore to result in very substantial excitations of C−H stretching vibrations, which explains the very significant broadening observed experimentally for this level, in both UPS and PIES.

The last feature that the EED simulation of Figure 1c shows is a band (**19**) at an electron energy of ca. 3.0 eV, which, according to the ADC(3)/cc-pVDZ results, dominantly relates to shake-up lines produced by ionization of an orbital (8a) which extends fully in phase outside the molecular surface (Figure 2). It is known that the EED model tends to underestimate the relative PIES of ionization bands derived from such orbitals,[27,28] a fact which a comparison of Figures 1b and 1c confirms.

B. Experimental and Theoretical Characterization of the Anisotropies of the Interaction Potential of He*(2^3S) around Biphenyl. The slope parameters (m) characterizing the collision-energy dependence of partial ionization cross sections (CEDPICS) obtained from the 2D-PIES measurements on biphenyl

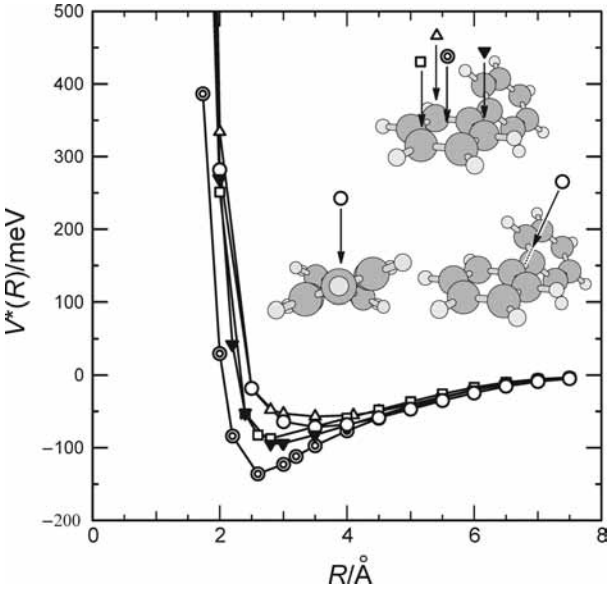

Figure 6. Interaction potential curves $V^*(R)$ for biphenyl and Li along various direction approaches. R is the distance between Li and C atoms, or between Li and the center of the phenyl ring or the C−C single bond.

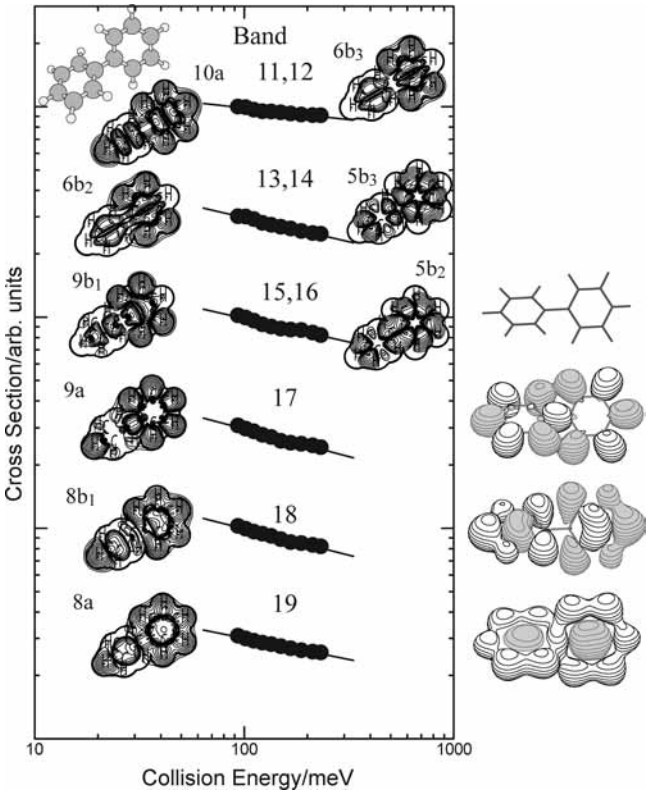

Figure 7. Collision-energy dependence of partial ionization cross sections of biphenyl with He*(2^3S) metastable atoms for bands 11−19.

in the gas phase have also been reported in Table 1. These slope parameters have been obtained by means of a least-squares method for collision energies ranging from 90 to 235 meV. He*-(2^3S) collision-energy-resolved Penning ionization electron spectra (CERPIES) of biphenyl are shown in Figure 4 for collision energies of ∼90 (dashed curve), ∼120 (solid curve), ∼150 (broken curve), and ∼200 meV (dotted curve). The CEDPICS of biphenyl are further displayed as log E_c vs log σ plots in Figure 5. These CEDPICS plots have been obtained from 2D-PIES measurements within an appropriate range of electron energies, typically in electron energy intervals equal to the resolution of the spectrometer, i.e., ∼250 meV, in order to avoid contamination from neighboring bands. Electron-density contour maps of σ orbitals are also shown on a plane including a phenyl group. For π orbitals electron-density maps have been plotted on a plane at a height of 1.7 Å above the plane including one of the two phenyl groups along with the 3D plots visualized by MOLDEN.[68] In these plots thick solid curves indicate the repulsive molecular surface approximated by van der Waals radii. At last, Figure 6 provides the interaction potential-energy curves $V^*(R)$ calculated at the MP2/6-31G level as a function of the distance R between the model Li probe and selected target points in the molecule along various direction approaches.

The partial ionization cross sections of the π-ionization channels are characterized by strongly negative collision-energy dependencies (Figure 5), which demonstrate on experimental grounds that the potential-energy surface describing the interaction between the molecule and the approaching He* probe is strongly attractive around the π-orbital region. The slope values ($m = -0.34$ to -0.45) obtained from the collision-energy dependence of the Penning π-ionization cross sections of biphenyl are similar to those previously inferred for the π levels of benzene ($m = -0.32$ or -0.34).[62,63,69] In agreement with these observations, strongly attractive potential wells are found from our potential calculations (Figure 6) when the Li(2^2S) model probe approaches the π-orbital region of biphenyl along axes that are perpendicular to the plane of one of the two phenyl rings. Among these model interaction curves, the deepest well is found when the approach follows an axis that intersects the center of one of these rings.

In contrast with the π levels, a much more limited collision-energy dependence is observed in CERPIES and CEDPICS for σ_{C-H} ionization bands such as bands **5**,**6** ($m = -0.03$). Therefore, the very limited slope parameter characterizing the CEDPICS of bands **4**,**5** indicates that the interaction potential that prevails around the σ_{C-H} bond region of aromatic hydrocarbons is more strongly repulsive. For the sake of comparison, it is worth recalling that slope parameters (m) ranging from +0.10 to −0.02 have been previously inferred from the CEDPICS of σ bands of benzene in effusive condition.[62,63,69] In contrast, the present 2D-PIES measurements on biphenyl yield CEDPICS slopes m around −0.10 for σ bands (bands **5**,**6** and **11**,**12**). Since the ADC(3) calculations demonstrate that the contribution of shake-up lines in the π-ionization band system is overall extremely limited at binding energies larger than 13 eV, the more strongly negative collision-energy dependence of σ cross sections can be ascribed to a stronger deflection of He* trajectories by enhanced attractive interactions at larger distances around the phenyl groups. Indeed, slope parameters around −0.1 have also previously been found for the CEDPICS characterizing the σ-ionization bands of naphthalene ($C_{10}H_8$).[70] For the sake of comparison, slope parameters around −0.2 have been inferred from the CEDPICS measured for the σ-ionization bands of anthracene ($C_{14}H_{10}$).[70] Considering all results obtained so far for benzene, naphthalene, anthracene, and biphenyl, these variations in the collision-energy dependence of Penning ionization cross sections indicate that the affinity of large π-conjugated molecules toward an impinging electrophilic species such as He*(2^3S) increases with system size as a result of an enhancement of the polarizability and electron-donating (metallic) nature of these aromatic systems, an observation which can ultimately be related to closure of the HOMO−

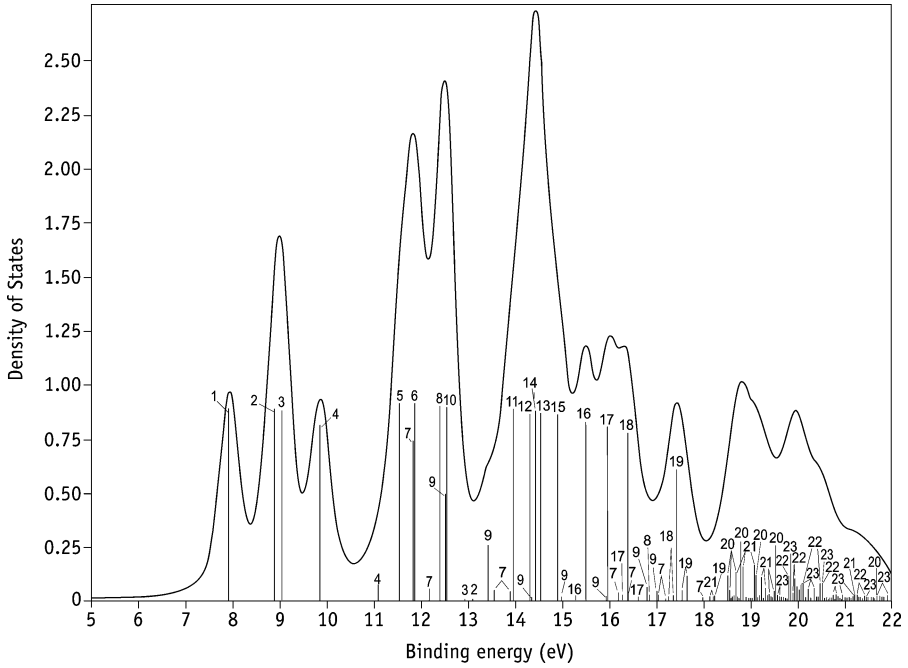

Figure 8. ADC(3)/cc-pVDZ ionization spectrum of the planar (first-order saddle-point) form (D_{2h}) of biphenyl (spike spectra and convoluted densities of states as a function of binding energies). See Table 2 for a detailed orbital assignment and the available Supporting Information for a comparison with an ADC(3)/6-31G simulation.

LUMO band gap and significant enhancements of electron-correlation effects (see ref 21 in particular). In line with this, a previous comparative PIES study of ethylene derivatives has also shown that the strength of the attraction forces between the molecular target and the He*(2^3S) probe very substantially increases as the ionization energy of an electron in the HOMO decreases.[71]

The $\pi_6-\pi_3$ and $\pi_2-\pi_1$ orbitals of biphenyl can be regarded as in-phase or out-of-phase combinations of the $1e_{1g}$ and $1a_{2u}$ orbitals of benzene, respectively. Since biphenyl has a nonplanar structure in the gas phase, the electron-density distributions of π orbitals are spatially rather intricate. In addition, the calculated potential curves show that due to enhanced steric interactions the central C−C bond is much less easily accessible than the centers of the phenyl rings (Figure 6). Some subtle differences in the CEDPICS characteristics of the three outermost π bands (**1**−**4**) are worth therefore a more detailed analysis. On the other hand, the ionization bands relating to the $8b_2$ (**7**, π_2) and $7b_3$ (**9**, π_1) orbitals overlap with σ-ionization bands and are therefore less easy to characterize. The CEDPICS of the 12a and $11b_1$ (**2**,**3**) ionization channels (π_4, π_5) have a slope parameter $m = -0.45$, compared with values of $m = -0.34$ and -0.42 for slopes characterizing the CEDPICS of the $9b_2$ (**1**, π_6) and $9b_3$ (**4**, π_3) ionization bands, respectively.

In Figure 5 we separately display the collision-energy dependence of the partial ionization cross sections (CEDPICS) of the shoulder (**S**) observed at an ionization energy around 13.2 eV in the He*(2^3S) PIES spectrum of Figure 1. The dependence of the cross sections is markedly negative ($m = -0.40$), which confirms the suggestion that this shoulder relates to the π-band system as a $\pi^{-2}\pi^{*+1}$ satellite of orbital $7b_3$ (**9**, π_1) (Table 1, Figure 3) rather than to the vibrational tail of the nearest and σ-one-electron ionization line derived from orbital $10b_1$ (**10**) at ~12.7 eV.

C. Conformational Fingerprints in the UPS and PIES Measurements on Biphenyl. The ADC(3)/cc-pVDZ result obtained for the planar first-order saddle-point form of biphenyl is displayed as a spike spectrum and convoluted densities of states in Figure 8. In Figure 9 we provide the He I UV and Ne* PIES photoelectron spectra which Kubota et al.[17] obtained from polycrystalline and amorphous thin films of biphenyl of about 10 nm thickness and deposited at temperatures of 170 and 109 K on a copper substrate, respectively. A simulation of PIES measurements on the planar form of biphenyl with gas-phase resolution is provided further in Figure 10 for the sake of comparison. The reader is referred to Table 2 for a quantitative assignment of these spectra and a comparison with ADC(3) and OVGF results. Most of the observations that were previously made regarding the accuracy of the computed one-electron ionization energies as well as the significance of OVGF pole strengths smaller than 0.85 are still valid and will not be repeated here.

A comparison with the theoretical simulations in Figure 3 indicates that many bands in the gas-phase ionization spectrum of biphenyl are rather sensitive to an alteration of the twist angle between the two phenyl rings. According to these simulations one of the most significant structural fingerprints for the planar first-order saddle-point form versus the twisted energy minimum form pertains to the relative energy location of the ionization bands relating to the σ orbitals **17**, **18**, and **19**. Very clearly, the UPS and PIES gas-phase measurements at electron-binding energies ranging from 15 to 18 eV are completely incompatible with the simulations drawn from a planar structure.

Compared with the situation that prevails in the gas phase, at least one structural fingerprint of the planar form is clearly apparent in the UPS and Ne* (PIES) (Figure 9) measurements performed on polycrystalline thin films of biphenyl deposited (or annealed) at 170 K.[17] The ADC(3) and OVGF results indicate that, by comparison with the twisted energy minimum form, planarity induces a significant increase, by about 0.4 eV, of the energy spreading of the four outermost π bands (see also Figure 2a), an observation which fully matches the experimental data for these layers.[17] These results demonstrate, therefore, on further spectroscopic grounds that the thermodynamically most stable configuration of biphenyl in an optimally relaxed crystalline network is planar at room temperature. In contrast, upon

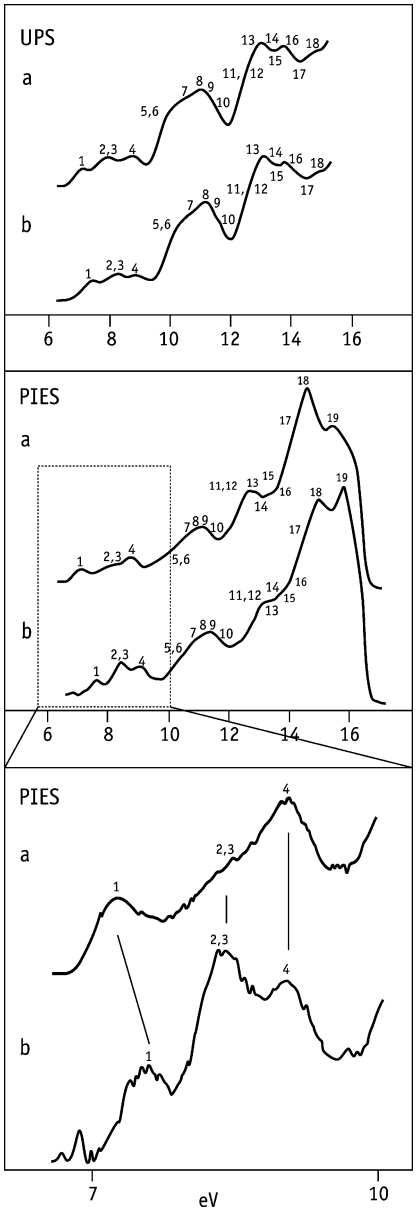

Figure 9. Assignment of the UPS and Ne* PIES measurements by Kubota et al.[17] on (a) polycrystalline and (b) amorphous layers of biphenyl deposited on copper at temperatures of 170 and 107 K, respectively.

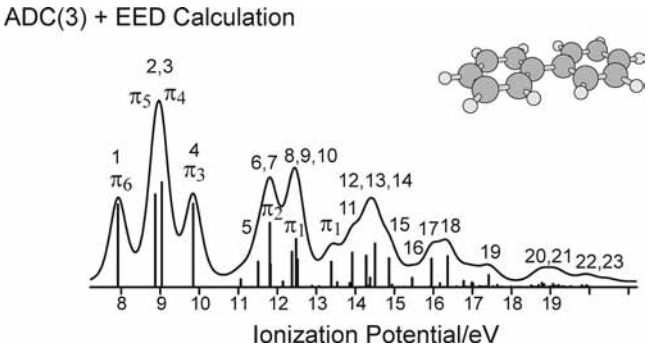

Figure 10. He*(2^3S) Penning ionization spectra simulated upon EED model cross sections, and the ADC(3)/cc-pVDZ results for the planar (D_{2h}) first-order saddle-point form of biphenyl.

both UPS and Ne* (PIES) measurements, it appears that the energy spreading of the four outermost π bands obtained from the film deposited at 109 K is very similar to that found in the gas phase and from the ADC(3)/cc-pVDZ calculations on the twisted (D_2) form of biphenyl. This obviously corroborates the amorphous, i.e., disordered, nature of this film and indicates that within the very top layers that are effectively probed by means of UPS and Ne* PIES, biphenyl predominantly lies within a twisted configuration. Such views are consistent with the conclusions drawn from Kubota et al.[17] upon considering the very limited intensity of the Ne* PIES intensities measured from the sample annealed at 170 K for the π_4 and π_5 orbitals (**2**,**3**) compared with that found for the film originally deposited at 109 K. Considering the topology of these orbitals (see Figure 2), these intensity variations indicate that the longitudinal axes of the molecules of biphenyl are all (approximately) aligned perpendicular to the surface of the polycrystalline layers, whereas the molecules at the surface of the amorphous film are merely randomly oriented.[17]

Identification of conformational fingerprints at higher ionization energies is more difficult for the thin films because of the lower experimental resolution and extremely strong inelastic scattering background or solid-phase effects such as relatively strong π-stack intermolecular interactions, long-range electronic and geometrical relaxations, phonon broadenings, etc. For a comparison of ionization energies with simulations on an absolute energy scale one would also need to know the work function of the sample. As the latter is unknown, bands in these measurements are therefore assigned (Figure 9) from their relative location. Despite the complications inherent to the solid phase, we note nonetheless that, in line with the simulations displayed in Figures 1c and 10, significant differences for bands **18**,**19** in the PIES spectra (Figure 9) of the thin films prepared at 170 and 109 K are observed. More specifically, a significant lowering of the intensity of band **19** relative to that of band **18** from the 170 (polycrystalline) to 109 K (amorphous) samples corroborates the suggestion that within the outermost layers of these samples biphenyl molecules adopt planar (D_{2h}) and twisted (D_2) conformations, respectively.

V. Conclusions

We have reported on the PIES and CERPIES study of the valence electronic structure of biphenyl in the gas phase, up to electron-binding energies of 20 eV, in conjunction with exterior electron-density (EED) calculations of partial cross sections in Penning ionization experiments and one-particle Green's function (1p-GF) [OVGF and ADC(3)] calculations of the one-electron and shake-up ionization spectra of model twisted and planar conformations. In the present work Penning ionization intensities have been analyzed by means of the EED model and comparison with UPS measurements in the gas phase. The agreement between theory and experiment is satisfactory overall up to electron-binding energies of ~18 eV, despite the extremely challenging nature of this compound, namely, its high torsional flexibility around the central C−C bond, a strongly conjugated character, and a propensity therefore to undergo electronic as well as vibrational excitation processes upon ionization. Due to near energy degeneracies between a number of states, likely complications due to vibronic coupling transitions are expected at ionization energies around 12 and 14 eV. It would be worth studying explicitly the bands measured at these energies using nuclear multistate dynamics.[67]

Compared with the lines originating from σ orbitals, ionization lines belonging to the π-band system, including shake-up lines, have much larger Penning ionization cross sections due to their greater extent outside the molecular vdW surface. Due to the neglect of phase factors, the EED model tends, nonethe-

TABLE 2: Theoretical EED Values (%) and [ADC(3), OVGF, and Koopmans] Ionization Spectra Computed for the First-Order Planar Form of Biphenyl[a]

	MO	$IP_{ADC(3)/cc-pVDZ}$	$IP_{OVGF/cc-pVDZ}$	$IP_{HF/cc-pVDZ}$	EED
1	$2b_{2g}$ (π_6)	7.93 (0.871)	7.86 (0.890)	7.92	4.87
2	$1a_u$ (π_5)	8.89 (0.862)	8.74 (0.887)	9.05	5.51
3	$1b_{1g}$ (π_4)	9.05 (0.860)	8.92 (0.887)	9.24	6.25
4	$2b_{3u}$ (π_3)	9.86 (0.796), 11.08 (0.074)	9.75 (0.882)	10.26	5.37
5	$7b_{3g}$	11.52 (0.889)	11.31 (0.896)	12.85	1.46
6	$11a_g$	11.84 (0.885)	11.55 (0.892)	13.25	1.31
7	$1b_{2g}$ (π_2)	11.82 (0.645), 12.16 (0.056), 13.55 (0.050)	11.86 (0.818)	13.26	5.11
8	$7b_{2u}$	12.39 (0.880)	12.20 (0.891)	13.77	2.06
9	$1b_{3u}$ (π_1)	12.49 (0.484), 13.40 (0.254), 16.79 (0.062)	12.65 (0.808)	14.25	5.10
10	$10b_u$	12.53 (0.872)	12.35 (0.886)	13.98	1.62
11	$6b_{3g}$	13.93 (0.861)	13.79 (0.879)	15.54	2.06
12	$10a_g$	14.29 (0.845)	14.10 (0.874)	15.96	1.92
13	$6b_{2u}$	14.52 (0.846)	14.39 (0.877)	16.17	2.64
14	$5b_{3g}$	14.39 (0.854)	14.04 (0.870)	16.19	0.57
15	$9b_{1u}$	14.88 (0.843)	14.83 (0.871)	16.59	1.76
16	$5b_{2u}$	15.47 (0.808)	15.09 (0.854)	17.40	0.59
17	$9a_g$	15.96 (0.781)	15.88 (0.856)	17.92	1.86
18	$8b_{1u}$	16.38 (0.757)	16.29 (0.849)	18.35	2.10
19	$8a_g$	17.43 (0.597), 17.65 (0.110)	17.34 (0.837)	19.57	1.03
20	$7b_{1u}$	18.52 (0.112), 18.70 (0.128), 18.79 (0.265), 19.12 (0.082)	18.74 (0.822)	21.50	0.82
21	$4b_{3g}$	18.71 (0.098), 18.85 (0.148), 19.08 (0.166), 19.23 (0.105), 19.33 (0.051)	18.99 (0.820)	21.82	0.99
22	$4b_{2u}$	19.82 (0.109), 19.94 (0.115), 20.11 (0.061), 20.48 (0.078), 20.52 (0.059)	20.00 (0.798)	22.96	0.83
23	$7a_g$	19.84 (0.081), 19.99 (0.058), 20.07 (0.071), 20.36 (0.051), 20.52 (0.076)	20.06 (0.815)	23.19	0.52

[a] Ionization energies are in eV. Only the lines with a pole strength larger than 0.05 (in parentheses) are reported. See Supporting Information for a more detailed description of the above ADC(3)/cc-pVDZ ionization spectrum and a comparison with ADC(3)/6-31G results.

less, to underestimate the relative intensity of fully bonding orbitals compared with orbitals characterized by a rich nodal structure. It would be worth improving on this model by explicitly accounting for the overlap between the 1s orbitals of the impinging He* atoms and the target molecular orbitals within a model employing thermostatistical mechanics[72] or classical dynamical calculations[73] based on quantum-chemical potential-energy surfaces for computing and integrating the results of different collision pathways rather than using rigid van der Waals boundary surfaces.

As a byproduct of the present study, a comparison of ADC(3) simulations with the PIES and UPS measurements performed by Kubota and co-workers[17] on thin films of biphenyl deposited at 170 and 109 K on copper demonstrates that biphenyl molecules lying at the surface of polycrystalline layers adopt predominantly a planar configuration, whereas within an amorphous sample most molecules have twisted structures similar to that prevailing in the gas phase. These conclusions have been drawn on the very reasonable assumption that, although they may change the ionization threshold of biphenyl by a few tenths of an electronvolt (see a previous study of the ionization threshold of oligoacenes at the confines of nonrelativistic quantum mechanics[21]), geometrical relaxation effects and further improvements of the quality of the basis set should influence the outermost electron-binding energies of the twisted and planar forms in very similar ways, considering that these forms have comparable HOMO−LUMO band gaps (which, at the HF/cc-pVDZ level, amount to 10.8 and 10.3 eV, respectively).

Acknowledgment. This work was supported by a Grant in Aid for Scientific Research from the Japanese Ministry of Education, Culture, Sports, Science and Technology. The quantum chemical calculations of EED cross sections and intermolecular interaction potentials have been performed at the Research Center for Computational Science, Okazaki National Research Institutes. All OVGF and ADC(3) calculations have been performed on an ES40 Compaq workstation at Hasselt University (formerly known as the Limburgs Universitair Centrum). M.S.D. acknowledges financial support and travel money from the FWO_Vlaanderen, the Flemish branch of the national science foundation of Belgium. S.K. is a Ph.D. grant holder of the *Bijzonder OnderzoeksFonds* of Hasselt University.

Supporting Information Available: Detailed ADC(3)/6-31G, ADC(3)/6-31G*, and ADC(3)/cc-pVDZ results along with simulated ionization spectra for the twisted and planar forms of biphenyl. This material is available free of charge via the Internet at http://pubs.acs.org.

References and Notes

(1) (a) Carreira, L. A.; Towns; T. G. *J. Mol. Struct.* **1977**, *41*, 1. (b) Bree, A.; Edelson, M. *Chem. Phys. Lett.* **1977**, *46*, 500.
(2) Bastiansen, O.; Samdal, S. *J. Mol. Struct.* **1985**, *128*, 115.
(3) Im, H.; Bernstein, E. R. *J. Chem. Phys.* **1988**, *88*, 7337.
(4) Takei, Y.; Yamaguchi, T.; Osamura, Y.; Fuke, K.; Kaya, K. *J. Phys. Chem.* **1988**, *92*, 577.
(5) In *Conjugated Polymers: The Novel Science and Technology of Highly Conducting and Nonlinear Optically Active Materials*; Brédas, J. L., Sillbey, R., Eds.; Kluwer: Dordrecht, The Netherlands, 1991.
(6) André, J. M.; Delhalle, J.; Brédas, J.-L. *Quantum Chemistry Aided Design of Organic Polymers−An Introduction to the Quantum Chemistry of Organic Polymers and Its Applications*; World Scientific Publishing Co. Pte. Ltd.: London, 1991.
(7) Arulmozhiraja, S.; Fujii, T. *J. Chem. Phys.* **2001**, *115*, 10589.
(8) (a) Erickson, M. D. *Analytical Chemistry of PCBs*; Butterworth: Boston, 1986. (b) Safe, S. *Polychlorinated Biphenyls−PCBs: Mammalian and Environmental Toxicology*; Springer-Verlag: Berlin, 1987.
(9) Keaton, T. E.; Lippincott, E. R. *Spectrochim. Acta* **1959**, *15*, 627.
(10) Fukui, K. *Theory of Orientation and Stereoselection*; Springer-Verlag: Berlin, 1975.
(11) Weigold, E.; McCarthy, I. E. *Electron Momentum Spectroscopy*; Kluwer Academic/Plenum Publishers: New York, 1999.
(12) (a) Čermák, V. *J. Chem. Phys.* **1966**, *44*, 3781. (b) Niehaus, A. *Adv. Chem. Phys.* **1981**, *45*, 399. (c) Yencha, A. J. *Electron Spectroscopy: Theory, Technique, and Applications*; Brundle, C. R., Baker, A. D., Eds.; Academic: New York, 1984; Vol. 5.
(13) (a) Suzuki, H. *Bull. Chem. Soc. Jpn.* **1959**, *32*, 1340. (b) Lim, E. C.; Li, Y. H. *J. Chem. Phys.* **1970**, *52*, 6416. (c) Eaton, V. J.; Steele, D. *J. Chem. Soc., Faraday Trans. 2* **1973**, *69*, 1601. (d) Murakami, J.; Ito, M.; Kaya, K. *J. Chem. Phys.* **1981**, *74*, 6505. (e) Tsuzuki, S.; Uchimaru, T.; Matsumura, K.; Mikami M.; Tanabe, K. *J. Chem. Phys.* **1999**, *110*, 2858.
(14) (a) Hargreaves, A.; Rizvi, S. H. *Acta Crystallogr.* **1962**, *15*, 365. (b) Charbonneau, G.-P.; Delugeard, Y. *Acta Crystallogr., Sect. B: Struct. Crystallogr. Cryst. Chem.* **1977**, *B33*, 1586. (c) Cailleau, H.; Baudour, J.

L.; Zeyen, C. M. E. *Acta Crystallogr., Sect. B: Struct. Crystallogr. Cryst. Chem.* **1979**, *B35*, 426.
(15) Almenningen, A.; Bastiansen, O.; Fernholt, L.; Cyvin, B. N.; Cyvin, S. J.; Samdal, S. *J. Mol. Struct.* **1985**, *128*, 59.
(16) (a) Pignataro, S.; Mancini, V.; Ridyard J. N. A.; Lempka, H. J. *Chem. Commun.* **1971**, 142. (b) Maier, J. P.; Turner, D. W. *Faraday Discuss. Chem. Soc.* **1972**, *54*, 149.
(17) Kubota, H.; Munakata, T.; Hirooka, T.; Kuchitsu, K.; Harada, Y. *Chem. Phys. Lett.* **1980**, *74*, 409.
(18) Hotop, H.; Niehaus, A. *Z. Phys.* **1969**, *228*, 68.
(19) See, e.g.: Szabo, A.; Ostlund, N. S. *Modern Quantum Chemistry: Introduction to Advanced Electronic Structure Theory*; Macmillan Publishing Co., Inc.: New York, 1982.
(20) (a) Cederbaum, L. S.; Domcke, W. *Adv. Chem. Phys.* **1977**, *36*, 205. (b) von Niessen, W.; Schirmer, J.; Cederbaum, L. S. *Comput. Phys. Rep.* **1984**, *1*, 57. (c) Ortiz, J. V. *J. Chem. Phys.* **1988**, *89*, 6348. (d) Zakrzewski, V. G.; von Niessen, W. *J. Comput. Chem.* **1993**, *14*, 13.
(21) Deleuze, M. S.; Claes, L.; Kryachko, E. G.; Francois, J.-P. *J. Chem. Phys.* **2003**, *119*, 3106.
(22) (a) Deleuze, M. S.; Cederbaum, L. S. *Int. J. Quantum Chem.* **1997**, *63*, 465. (b) Deleuze, M. S.; Cederbaum, L. S. *Adv. Quantum Chem.* **1999**, *35*, 77.
(23) (a) Deleuze, M. S.; Giuffreda, M. G.; Francois, J.-P.; Cederbaum, L. S. *J. Chem. Phys.* **1999**, *111*, 5851. (b) Deleuze, M. S.; Giuffreda, M. G.; Francois, J.-P.; Cederbaum, L. S. *J. Chem. Phys.* **2000**, *112*, 5325. (c) Deleuze, M. S.; Giuffreda, M. G.; Francois, J.-P. *J. Phys. Chem. A* **2002**, *106*, 5626.
(24) (a) Deleuze, M. S.; Trofimov, A. B.; Cederbaum, L. S. *J. Chem. Phys.* **2001**, *115*, 5859. (b) Deleuze, M. S. *J. Chem. Phys.* **2002**, *116*, 7012. (c) Deleuze, M. S. *J. Phys. Chem. A* **2004**, *108*, 9244.
(25) Deleuze, M. S.; Pang, W. N.; Salam, A.; Shang, R. C. *J. Am. Chem. Soc.* **2001**, *123*, 4049.
(26) Ohno, K.; Mutoh, H.; Harada, Y. *J. Am. Chem. Soc.* **1983**, *105*, 4555.
(27) Ohno, K.; Matsumoto, S.; Harada, Y. *J. Chem. Phys.* **1984**, *81*, 4447.
(28) Ohno, K.; Harada, Y. Penning Ionization: the Outer Shape of Molecule. In *Theoretical Models of Chemical Bonding, Part 3*; Maksič, Z. B., Ed.; Springer-Verlag: Berlin, 1991; pp 199−233.
(29) Pauling, L. *The Nature of the Chemical Bond*; Cornell University: Ithaca, NY, 1960.
(30) Niehaus, A. *Ber. Bunsen-Ges. Phys. Chem.* **1973**, *77*, 632.
(31) Rothe, E. W.; Neynaber, R. H.; Trujillo, S. M. *J. Chem. Phys.* **1965**, *42*, 3310.
(32) Hotop, H. *Radiat. Res.* **1974**, *59*, 379.
(33) Haberland, H.; Lee, Y. T.; Siska, P. E. *Adv. Chem. Phys.* **1981**, *45*, 487.
(34) Mitsuke, K.; Takami, T.; Ohno, K. *J. Chem. Phys.* **1989**, *91*, 1618.
(35) Ohno, K.; Yamakado, H.; Ogawa, T.; Yamata, T. *J. Chem. Phys.* **1996**, *105*, 7536.
(36) Ohno, K.; Takami, T.; Mitsuke, K.; Ishida, T. *J. Chem. Phys.* **1991**, *95*, 918.
(37) Handy, N. C.; Marron, M. T.; Silverstone, H. J. *Phys. Rev.* **1969**, *180*, 45.
(38) Morrell, M. M.; Parr, R. G.; Levy, M. *J. Chem. Phys.* **1975**, *62*, 549.
(39) Schirmer, J.; Cederbaum, L. S.; Walter, O. *Phys. Rev. A* **1983**, *28*, 1237.
(40) Schirmer, J.; Angonoa, G. *J. Chem. Phys.* **1989**, *91*, 1754.
(41) Weikert, H.-G.; Meyer, H.-D.; Cederbaum, L. S.; Tarantelli, F. *J. Chem. Phys.* **1996**, *104*, 7122.
(42) Cederbaum, L. S.; Hohlneicher, G.; Peyerimhoff, S. *Chem. Phys. Lett.* **1971**, *11*, 421.
(43) Pickup, B. T.; Goscinski, O. *Mol. Phys.* **1973**, *26*, 1013.
(44) Ohrn, Y.; Born, G. *Adv. Quantum Chem.* **1981**, *13*, 1.
(45) Ortiz, J. V. In *Computational Chemistry: Reviews of Current Trends*; Leszczyinski, J., Ed.; World Scientific: Singapore, 1997; Vol. 2, p 1.
(46) Deleuze, M. S. *Int. J. Quantum Chem.* **2003**, *93*, 191.
(47) Deleuze, M. S.; Scheller, M. K.; Cederbaum, L. S. *J. Chem. Phys.* **1995**, *103*, 3578.
(48) (a) Dunning, T. H. *J. Chem. Phys.* **1989**, *90*, 1007. (b) Kendall, R. A.; Dunning, T. H.; Harrison, R. J. *J. Chem. Phys.* **1992**, *96*, 6796.
(49) (a) Becke, A. D. *J. Chem. Phys.* **1993**, *98*, 5648. (b) Lee, C.; Yang, W.; Parr, R. G. *Phys. Rev. B* **1988**, *37*, 785.
(50) Martin, J. M. L.; El-Yazal, J.; François, J.-P. *Mol. Phys.* **1995**, *86*, 1437.
(51) Schmidt, M. W.; Baldridge, K. K.; Jensen, J. H.; Koseki, S.; Gordon, M. S.; Nguyen, K. A.; Windus, T. L.; Elbert, S. T. *QCPE Bull.* **1990**, *10*, 52.
(52) (a) Liu, B. In *Numerical Algorithms in Chemistry, Algebraic Methods;* LBL-8158; Lawrence Berkeley Laboratory. (b) Tarantelli, F.; Sgamellotti, A.; Cederbaum, L. S.; Schirmer, J. *J. Chem. Phys.* **1987**, *86*, 2201.
(53) See Supporting Information for a detailed comparison of ADC(3)/6-31G, ADC(3)/6-31G*, and ADC(3)/cc-pVDZ data or convoluted spectra (fwhm = 0.5 eV).
(54) Frisch, M. J.; et al. *GAUSSIAN 98* (Revision A.7); Gaussian Inc.: Pittsburgh, PA, 1998.
(55) Takami, T.; Ohno, K. *J. Chem. Phys.* **1992**, *96*, 6523.
(56) Gardner, J. L.; Samson, J. A. R. *J. Electron Spectrosc. Relat. Phenom.* **1976**, *8*, 469.
(57) Kimura, K.; Katsumata, S.; Achiba, Y.; Yamazaki, T.; Iwata, S. *Handbook of He I Photoelectron Spectra of Fundamental Organic Molecules*; Japan Scientific Press: Tokyo, 1981.
(58) (a) Illenberger, E.; Niehaus, A. *Z. Phys. B* **1975**, *20*, 33. (b) Woodard, M. R.; Sharp, R. C.; Seely, M.; Muschlitz, E. E., Jr. *J. Chem. Phys.* **1978**, *69*, 2978. (c) Parr, T.; Parr, D. M.; Martin, R. M. *J. Chem. Phys.* **1982**, *76*, 316. (d) Appolloni, L.; Brunetti, B.; Hermanussen, J.; Vecchiocattivi, F.; Volpi, G. G. *J. Chem. Phys.* **1987**, *87*, 3804.
(59) Kishimoto, N.; Aizawa, J.; Yamakado, H.; Ohno, K. *J. Phys. Chem. A* **1997**, *101*, 5038.
(60) Kishimoto, N.; Yamakado, H.; Ohno, K. *J. Phys. Chem.* **1996**, *100*, 8204.
(61) Tian, S. X.; Kishimoto, N.; Ohno, K. *J. Phys. Chem. A* **2002**, *106*, 7714.
(62) Yamakita, Y.; Yamauchi, M.; Ohno, K. *Chem. Phys. Lett.* **2000**, *322*, 189.
(63) Yamazaki, M.; Maeda, S.; Kishimoto, N.; Ohno, K. *J. Chem. Phys.* **2005**, *122*, 044303.
(64) Kishimoto, N.; Ohno, K. *J. Phys. Chem. A* **2000**, *104*, 6940.
(65) Masuda, S.; Aoyama, M.; Ohno, K.; Harada, Y. *Phys. Rev. Lett.* **1990**, *65*, 3257.
(66) Knippenberg, S.; Nixon, K. L.; Brunger, M. J.; Maddern, T.; Campbell, L.; Trout, N.; Wang, F.; Newell, W. R.; Deleuze, M. S.; Francois, J.-P.; Winkler, D. A. *J. Chem. Phys.* **2004**, *121*, 10525.
(67) (a) Köppel, H.; Cederbaum, L. S.; Domcke, W. *J. Chem. Phys.* **1988**, *89*, 2023. (b) Döscher, M.; Köppel, H.; Szalay, P. G. *J. Chem. Phys.* **2002**, *117*, 2645. (c) Köppel, H.; Döscher, M.; Bâldea, I.; Meyer, H.-D.; Szalay, P. G. *J. Chem. Phys.* **2002**, *117*, 2657.
(68) Schaftenaar, G. CAOS/CAMM Center, The Netherlands, 1991.
(69) Horio, T.; Maruyama, R.; Kishimoto, N.; Ohno, K. *Chem. Phys. Lett.* **2004**, *384*, 73.
(70) Yamauchi, M.; Yamakita, Y.; Yamakado, H.; Ohno, K. *J. Electron Spectrosc. Relat. Phenom.* **1998**, *88*−*91*, 155.
(71) Yamakado, H.; Okamura, K.; Ohshimo, K.; Kishimoto, N.; Ohno, K. *Chem. Lett.* **1997**, 269.
(72) Suggestion by M. S. Deleuze.
(73) (a) Ogawa, T.; Ohno, K. *J. Chem. Phys.* **1999**, *110*, 3773. (b) Ohno, K. *Bull. Chem. Soc. Jpn.* **2004**, *77*, 887.